Quantum Electronics **50** (12) 1126–1133 (2020)

https://doi.org/10.1070/QEL17412

Generation of high-power few-cycle femtosecond IR pulses by double-chirp parametric amplification

S.A. Frolov, V.I. Trunov

Abstract. **We present an energy scalable configuration for the generation of high-power few-cycle femtosecond IR pulses based on the sequential parametric amplification of chirped radiation pulses at the idler (0.86 μm) and signal (1.39 μm) wavelengths from the multi-terawatt femtosecond laser system made at the Institute of Laser Physics, Siberian Branch of the Russian Academy of Sciences (ILP SB RAS). The configuration under consideration involves the sequential production of radiation pulses with centre wavelengths of 2.24, 3.56, and 7.25 μm. The conditions are determined for the generation of few-cycle pulses with a terawatt peak power in the 3.56 μm (15.8 fs, 1.5 cycles) and 7.25 μm (17.2 fs, shorter than one cycle) domains. The phase transfer between signal and idler waves in the double-chirp parametric amplification is investigated for the first time.**

Keywords: *femtosecond pulses, IR range, optical parametric amplification, few-cycle pulses, double-chirp amplification.*

1. Introduction

Femtosecond laser systems that generate high-energy few-cycle IR pulses are tools in demand for the production of UV and soft X-ray radiation sources by high-order harmonic generation [1] as well as for the production with their use of high-power isolated attosecond pulses [2]. This type of IR laser systems may be implemented using double-chirp parametric amplifiers pumped by picosecond lasers [3, 4]. To date, femtosecond pulses are obtained in the mid-IR range with energies up to 31 mJ (duration: 70 fs) in the 3.3 μm domain [5], 1 mJ (duration: 80 fs) in the 5 μm domain [6], and 0.2 mJ (duration: 180 fs) in the 7 μm domain [7]. Ultra-wideband parametric amplification schemes are required for generating few-cycle pulses in this range [8]. Different nonlinear-optical techniques of compressing amplified pulses to ultimately short pulses are also considered and analysed [9, 10]. Under parametric amplification it was possible to experimentally generate sub-cycle pulses in the 4 μm domain (duration: 12.4 fs, 0.88 cycle; energy: 33 μJ) [11]. Under parametric amplification in a GaSe crystal pumped in the 2-μm domain, ultra-wideband radiation of microjoule energy was generated in the 4.5–13.3 μm domain, which is supposed to be compressed into a pulse with an extremely short duration in [12].

An advantage of a double-chirp parametric amplifier consists in that this approach permits doubling the spectral width of the generated idler wave in comparison with that under a single chirping, provided that the parametrically amplified waves have chirps of opposite sign [13]. Usually, there is an optimal ratio between the durations of chirped pulses in the parametric amplification [14], but in our case, the durations of these pulses are determined by the features of their formation in the proposed configuration.

S.A. Frolov Institute of Laser Physics, Siberian Branch, Russian Academy of Sciences, prosp. Akad. Lavrent'eva, 13/3, 630090 Novisibirsk, Russia; e-mail: stanislav.a.frolov@gmail.com;
V.I. Trunov Institute of Laser Physics, Siberian Branch, Russian Academy of Sciences, prosp. Akad. Lavrent'eva 13/3, 630090 Novisibirsk, Russia; Novosibirsk State University, ul. Pirogova 2, 630090 Novisibirsk, Russia; Novosibirsk State Technical University, prosp. Karla Marksa 20, 630073 Novosibirsk, Russia.

Received 27 July 2020; revision received 16 September 2020
Kvantovaya Elektronika **50** (12) 1126–1133 (2020)
Translated by E.N. Ragozin

2. Development of the optimal scheme for the generation of high-power few-cycle IR femtosecond pulses

The proposed scheme for the production of high-power few-cycle IR femtosecond pulses involves the sequential parametric amplification of chirped radiation pulses at the idler and signal wavelengths (transform-limited duration: 20 fs) from the multi-terawatt femtosecond laser system implemented at the ILP SB RAS, which operates at a pulse repetition rate of 10 Hz [15]. Beginning with the signal wave with the centre wavelength equal to 0.86 μm and the idler one at a wavelength of 1.39 μm, radiation pulses with centre wavelengths of 2.24, 3.56, and 7.25 μm are sequentially generated in the configuration. In comparison with difference frequency generation, this approach makes it possible to generate amplified few-cycle IR femtosecond pulses of higher energy at the expense of a complication of the experimental scheme.

We also note that the timing of the pulses interacting at each amplification stage is automatically maintained in the configuration under development. The timing accuracy is determined by the accuracy of the precision timing scheme of the laser system made for producing the pulses of pump radiation (532 nm) and the amplified wave (0.86 μm) as well as by the initial timing accuracy of about 0.3–0.5 ps [16].

Direct calculation of noncollinearity and phase-matching angles by analytical techniques for each stage does not permit selecting their optimal values owing to the strong interdependence of the stages determined by the amplified pulse spectrum. That is why these values are selected simultaneously for all stages by maximising the peak power of the amplified pulse at the last stage. Optimisation was carried out by the simplex method. Numerical simulations were carried out with the use of equations outlined in Refs [17, 18]. Selected for a merit function, as noted above, was the peak power of amplified pulses in turn at each stage. The developed scheme is shown in Fig.1.

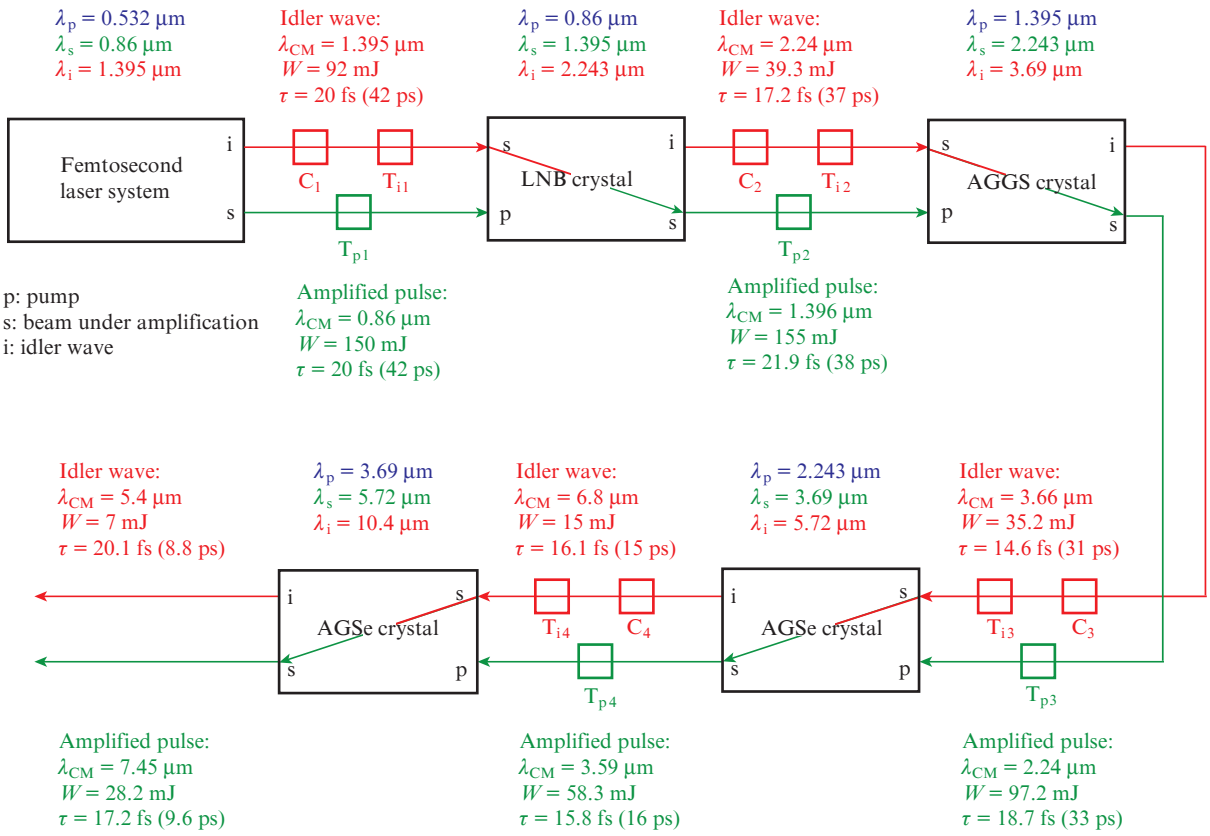

Figure 1. (Colour online) Schematic of sequential parametric amplification of femtosecond IR pulses. Letters C and T with subscripts denote spectral-angular chirp compensators and telescopes, respectively; λ_{CM} is the centre-of-mass spectrum wavelength.

Although many nonlinear-optical crystals are suited for mid-IR radiation generation, their practical use is limited either the available apertures or by a low breakdown threshold caused by the two-photon absorption of the pump radiation [19]. Furthermore, few crystals maintain broadband amplification at the wavelengths selected. In the designed configuration, in the parametric stages with vector geometry and type-I phase matching we plan the use of LNB ($MgO:LiNbO_3$) crystals at the first stage, AGGS ($AgGaGeS_4$) crystals [20–22] at the second stage, and next AGSe ($AgGaSe_2$) crystals [14]. The AGSe crystals are chosen for the third and fourth stages, because they possess the highest effective nonlinearities among the available crystals like AGS ($AgGaS_2$) and AGGS as well as an ultra-broadband spectral phase matching for comparable breakdown thresholds. The use of AGSe crystals in parametric amplifiers pumped at a wavelength of 1.064 μm is limited by its large two-photon absorption coefficient, which is significantly lower at wavelengths exceeding 1.4 μm [23].

The feasibility of producing radiation tunable in the domain 5–18 μm by generating difference frequencies in AGSe crystals was demonstrated in Refs [24, 25] for an output energy of about 1 nJ. The generation of broadband radiation in the domain 7–11 μm with efficiency up to 0.8% was realised for type-II phase matching in an AGSe crystal under pumping by 26-fs long pulses with a wavelength of about 2.1 μm [26]. The peak intensity of the pump pulses was as high as 200 GW cm^{-2}, which is equivalent to an intensity of over 6 GW cm^{-2} in terms of a 26-ps duration.

A comparison analysis of the properties of nonlinear-optical crystals transparent in the IR region [23] and suited for use in the configuration under development suggests that the selected crystals have the best characteristics, which provide retention of the spectral width of amplified signals under double chirping conditions. For the respective initial energies 150 and 90 mJ of the femtosecond radiations with centre wavelengths of 0.86 μm (signal wave) and 1.39 μm (idler wave), the expected pulse energies after parametric amplification stages are 155 mJ (duration: 21.6 fs) in the 1.39-μm domain, 95 mJ (duration: 17 fs) in the 2.24-μm domain, 56 mJ (duration: 15 fs) in the 3.56-μm domain, and 25 mJ (duration: 17 fs) in the 7.25-μm domain. The initial chirped 41.6-ps long pulses of the signal and idler waves have a Gaussian profile and have sixth- and fourth-order super-Gaussian spatial profiles, respectively. The requisite crystal parameters for each stage of optimal geometry, which is characterised by large noncollinearity angles, and for comparison, the parameters for small noncollinearity angles equal to 0.4° are collected in Table 1.

The noncollinearity angle α is measured from the pumping beam axis in the same direction as the phase-matching angle θ. Shown in Table 1 are data for a negative non-collinearity angle, since this scheme is less critical to deviations of angles α and θ. In what follows we consider it by default. Similar simulation data for the positive angle are lower by 0.5%–1% (the pulse duration is longer and the energy is lower), depending on the stage number, and we therefore believe that this configuration does not call for a detailed analysis.

Table 1. Optimal configuration parameters.

Stage	Transparency range/μm	Symmetry class	d_{eff}/pm V^{-1} (LNA)	d_{eff}/pm V^{-1} (SNA)	α/deg (LNA)	α/deg (SNA)	θ/deg (LNA)	θ/deg (SNA)	Crystal length/mm (LNA)	Crystal length/mm (SNA)	Crystal aperture/mm
1 (LNB)	0.33–5.5	3m	5.2	5.06	−7.68	−0.4	69.15	43.78	1.2	1.2	14
2 (AGGS)	0.5–13	mm2	8.45	4.28	−7.81	−0.4	90	35.9	2.7	4.9	23
3 (AGSe)	0.71–18	42m	33	22.3	−4.99	−0.4	90	42.46	1.3	2	19
4 (AGSe)	0.71–18	42m	33	21.5	−5.31	−0.4	90	40.58	2.2	2.6	16

Note: LNA stands for large noncollinearity angles, and SNA denotes small noncollinearity angles.

Parametric conversion for large noncollinearity angles provides an ultra-broad spectral amplification band as well as the possibility to use the maximal effective nonlinearity and the spatial separation of the amplified beams at short distances. As a rule, in the parametric amplification in the IR region, use is made of small noncollinearity angles [13, 26]. As suggested by the data presented in Table 1, the effective nonlinearity d_{eff} is significantly lower for small noncollinearity angles, especially so for the last three stages. Furthermore, for small noncollinearity angles, as shown in Fig. 2, the spectral band of parametric amplification is significantly narrower.

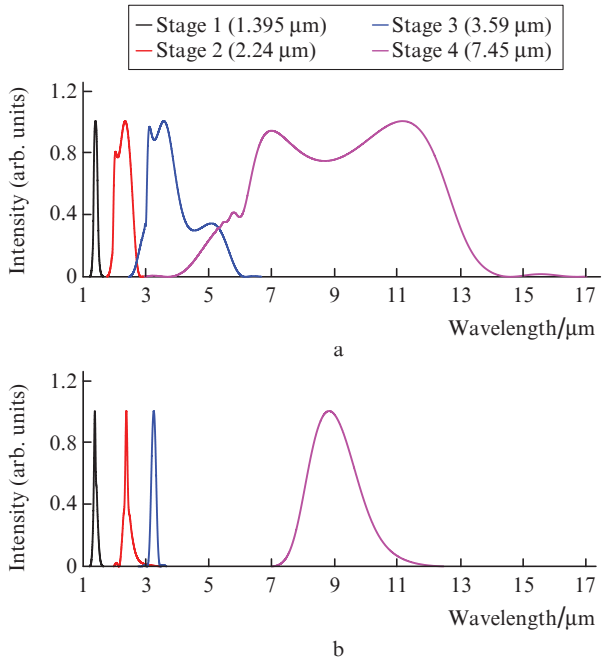

Figure 2. (Colour online) Spectra of amplified pulses in different IR domains for large noncollinearity angles (a) and for an angle of 0.4° (b).

As is well known, an angular chirp occurs in an idler wave at each stage of parametric amplification, which must be compensated both for subsequent amplification stages and for the compressor in the scheme under consideration.

For the crystals employed in the configuration, the angular chirp has the following values: 44.8–44.5 μrad nm^{-1} in the range 1.3–1.5 μm (input radiation), 136–130 μrad nm^{-1} in the range 1.9–2.7 μm (the idler wave of the first stage), 88.4–86.1 μrad nm^{-1} in the range 2.7–5.7 μm (the idler wave of the second stage), 31.7–30 μrad nm^{-1} in the range 4.5–13.5 μm (the idler wave of the third stage), and 19.8–21.2 μrad nm^{-1} in the range 4–13 μm (the idler wave of the fourth stage). These angular dispersions are easy to compensate for with an optical configuration comprising a telescope and a diffraction grating [27]. The residual spectral-angular chirp that has to be compensated for may be estimated proceeding from the fact that the angular range for the idler wave should be of the order of diffraction-limited divergence of the beams. According to the data of our numerical simulations, this chirp is 6 μrad nm^{-1} for the input radiation of the first stage, 1.2 μrad nm^{-1} for the second stage, 0.6 μrad nm^{-1} for the third one, and 0.3 μrad nm^{-1} for the fourth. After each stage the amplified idler radiation pulse can be compressed by the compressor to the ultimately short one for a residual angular chirp of less than 10 μrad nm^{-1}. The possibility of efficient compensation of the spectral-angular chirp of the idler wave in the domain of 3.1 μm and the generation of pulses with a duration of less than five field cycles (53 fs) was demonstrated in Ref. [28].

We also note that the amplified compressed idler radiation pulses have a high temporal contrast, which is mainly determined by the compressor parameters, and not by the parametric luminescence. This is due to the fact the parametric luminescence already present in the amplified signal wave is not transferred to the idler wave during its generation, which significantly improves its contrast. Therefore, the contrast of the generated pulses is independent on the contrast of the driving pulses at wavelengths of 0.86 and 1.395 μm. In the subsequent amplification of the idler wave, the gain is low (on the order of unity, for example, in the first stage it is 1.7) and does not result in a significant development of intrinsic parametric luminescence.

3. Analysis of amplified radiation parameters

The pulse energies, the peak pulse intensities (I_{peak}) in crystals, the spatial profile characteristics, the chirped (τ_{chirp})and compressed (τ_{comp}) pulse durations, as well as the spectrum centre-of-mass wavelengths (λ_{CM}) defined as the centre of mass of the frequency spectrum, i.e.

$$\lambda_{CM} = 2\pi c \int I(\omega)\mathrm{d}\omega \left[\int \omega I(\omega)\mathrm{d}\omega\right]^{-1},$$

at the output of each stage are collected in Table 2.

The initial diameter of the amplified (0.86 μm) and idler (1.359 μm) beams of the laser system developed at the ILP SB RAS, according to the results of experimental measurements, was assumed to be ~1 cm (full width at half height). The corresponding minimal requisite apertures of the nonlinear opti-

Table 2. Parameters of amplified pulses.

Stage	Wave	λ/μm	λ_{CM}/μm	Energy/mJ	I_{peak}/GW cm^{-2}	τ_{comp}*/fs	τ_{chirp}/ps	n**
1 (at input)	Amplified	1.395	1.395	91.9	3.20	20.1	41.6	4
	Pumped	0.860	0.860	149.5	4.80	20.1	41.6	6
1 (at output)	Amplified	1.395	1.396	154.9	5.71	21.9	38.4	5
	Idler	2.243	2.224	39.3	1.63	17.2	36.8	6
	Pumped	0.860	0.863	46.9	1.71	16.1	64.6	–
2 (at output)	Amplified	2.243	2.239	97.2	1.74	18.7	32.8	6.5
	Idler	3.690	3.665	35.2	0.72	14.6	31.4	6.5
	Pumped	1.395	1.400	61.7	0.99	18.1	49.7	–
3 (at output)	Amplified	3.690	3.587	58.3	1.67	15.8	16.0	6.5
	Idler	5.719	6.803	15.0	0.64	16.1	14.5	6
	Pumped	2.243	2.201	58.8	1.44	16.8	34.6	–
4 (at output)	Amplified	5.719	7.453	28.2	1.74	17.2	9.6	6
	Idler	10.4	5.375	7.0	0.61	20.1	8.8	6
	Pumped	3.960	3.766	38.5	1.80	14.9	7.1	–

* Duration of the pulsed compressed with compensation up to the fourth-order spectral phase term, inclusive.
** Degree of super-Gaussianity of the spatial profile: $f(r) \propto \exp[-2(r/w_0)^{2n}]$.

cal crystals for each stage were chosen in such a way that more than 99.998% of the radiation passed through the crystal, which corresponds to a size 1.35 times the beam diameter for the third- and higher-order super-Gaussian profiles.

It is noteworthy that the peak intensities, for instance in the domain 3.59 μm, are about the same after the third and fourth amplification stages because of the shortening of amplified chirped pulse duration from stage to stage. The pulse shortening is due to the simultaneous temporal chirp reduction with increasing stage number and with the pulse spectrum narrowing under amplification. At the last stage (duration: 9.6 ps), in particular, to retain the chirped pulse duration equal to 41.6 ps the spectrum width should be four times greater.

It is planned to employ telescopes with image transfer (see Fig. 1) with a magnification coefficient of 1.7 between the first and second amplification stages (T_{i2}, T_{p2}), with unit magnification between the second and third ones (T_{i3}, T_{p3}), and with a magnification coefficient of 0.95 between the third and the fourth (T_{i4}, T_{p4}). The maximise the pulse energy in the domain

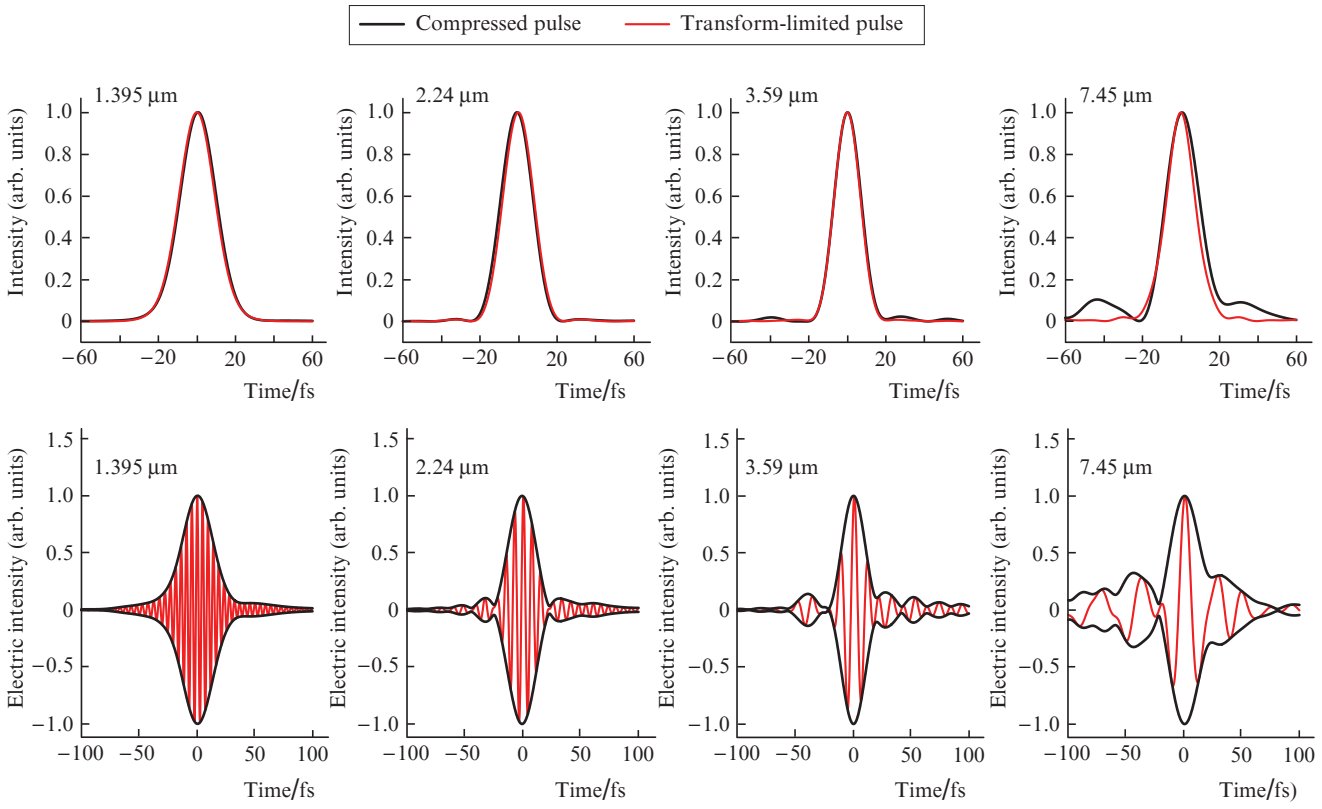

Figure 3. (Colour online) Temporal intensity profiles of compressed (with compensation up to the fourth-order spectral phase term, inclusive) and transform-limited pulses (upper row), as well as electric field distributions (lower row) in different spectral domains.

7.45 μm and, therefore, a terawatt-high power, use should be made of vacuumed versions of telescopes before the first and second stages.

In the scheme developed here, in the mid-IR it is possible to generate few-cycle pulses with durations shorter than one cycle (Fig. 3) by virtue of ultra-broadband phase matching for large noncollinearity angles in AGGS and AGSe crystals. In this configuration it is possible to scale up the energy of amplified IR pulses by increasing the energies of input pulses at the wavelengths 0.86 and 1.359 μm. Compressing positively chirped amplified pulses calls for the use of compressors with an internal telescope. The special features of using such compressor configurations to compress large-aperture amplified pulses in the IR region were comprehensively analysed in our earlier works [29, 30]. Determined in these papers were the main requirements imposed on the compressor components and the precision of their alignment.

The results of calculations for small noncollinearity angles are outlined in Table 3. One can see that the transform-limited pulse duration τ_{TL} is significantly longer for small noncollinearity angles, i.e. the width of the amplification spectrum is too small to maintain the high efficiency of amplification. This accounts for the significant shortening of the chirped pulse duration, which in turn results in a decrease in the degree of temporal overlap of the pulses and the consequential lowering of the energy of the amplified pulses.

Table 3. Parameters of amplified pulses for small noncollinearity angles at the outputs of the stages.

Stage	λ/μm	λ_{CM}/μm	Energy/mJ	τ_{TL}/fs	τ_{chirp}/ps
1	1.395	1.388	120	20.9	28.2
2	2.243	2.405	21.1	20.4	4.9
3	3.690	3.241	6.7	65.2	3.1
4	5.719	8.867	4.3	67.8	2.6

Also analysed was the influence of the mismatch between the noncollinearity and phase matching angles. Experimentally, this corresponds to the accuracy of adjusting the angles at which there propagate the pump radiation (the noncollinearity and phase matching angles vary in opposite directions) and the amplified beam (the noncollinearity angle changes). Angular deviations were introduced into the stages separately. The results are given in Fig. 4. The requirements for the tolerances of the angular adjustment of the beams at different stages are given in greater detail in Table 4.

As follows from the data presented in Table 4, in the scheme under consideration, the requirements on the accuracy of angular adjustment for AGSe crystals are lower than for LNB and AGGS crystals. This is due to the transition to noncritical phase matching at large noncollinearity angles and to the specific features of the optical dispersion properties of AGSe crystals. The low requirements for the accuracy of adjusting the angles for the last two stages lead to a decrease

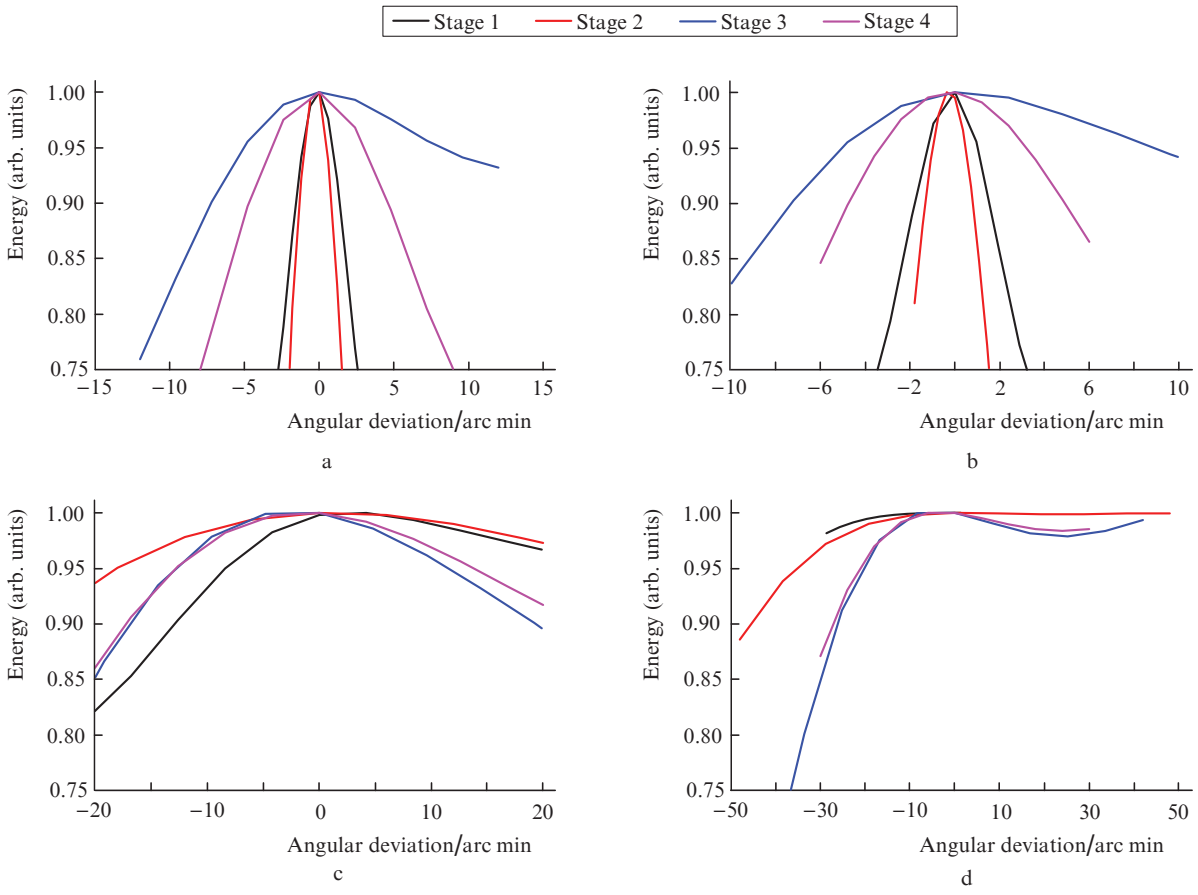

Figure 4. (Colour online) Dependences of the amplified pulse energy on the angular deviations in the sensitive plane of the pump beam (a, c) and in the plane of the amplified beam (b, d) at large noncollinearity angles (a, b) and at an angle of 0.4° (c, d) for all stages.

Table 4. Sensitivity to angular deviations of the propagation of the pump beam and the amplified beam in the phase-matching plane.

Stage	Sensitivity* when the gain lowers to 95%/arc min	Sensitivity* when the gain lowers to 90%/arc min	Crystal length/mm	α /deg
1	0.5 (1.2)	0.84 (1.8)	1.2	7.68
2	0.8 (1)	1.4 (1.3)	2.7	7.81
3	2.7 (5)	4.5 (7.3)	1.3	4.99
4	5 (3.3)	7.2 (4.8)	2.3	5.31
1	8 (33)	13 (40)	1.2	0.4
2	18 (33)	24 (45)	4.9	0.4
3	12.5 (20)	16.7 (26)	2	0.4
4	12.5 (20)	17 (27)	2.6	0.4

*The values are given for decreasing (increasing) the angle.

in the requirements for the angular stability of interacting pulses and, consequently, for the stability of all mechanical alignment devices.

The configuration with small noncollinearity angles makes it possible to simplify the compensation of the angular chirp, and is also characterised by a very low angular sensitivity. A disadvantage of this scheme is the longer duration of compressed amplified pulses and their low energy. Furthermore, a distance of at least 3 m is required to separate the amplified pulse and the idler wave.

Another important factor in achieving stability of the energy of the amplified pulses is the requirement for the accuracy of timing of the interacting pulses in the crystal at each stage. We obtained the following values for a 5% decrease in energy for stages from the first to the last: 16, 12, 5, and 2.3 ps, respectively. These stringent requirements are explained by the large width of the amplification spectrum, since the time shift also leads to a shift in the frequencies of the interacting waves due to the presence of a chirp. Due to saturation in the amplifier stages, the stability of the pulse energy turns out to be high in relation to the stability of the intensity at the front of the pump pulses. A further increase in the delay between pulses causes a rapid decrease in the amplified pulse energy by reducing the overlap area.

4. Idler and amplified wave phases after the stages of parametric double-chirp pulse amplification

To successfully compress the pulses after double-chirp parametric amplification, it is of importance to calculate the expansion coefficients of the residual spectral phase into a Taylor series after each stage. To do this, we write the Fourier transform of the chirped-pulse electric field $E(t)$ with phase φ expanded into the Taylor series about some central frequency ω_0 with coefficients φ_n, and in the resultant expression we perform integration by the method of stationary phase due to the high frequency of field oscillation:

$$E(t) \propto E_\omega(\omega_s(t))\exp\left\{i\sum_n \frac{\varphi_n}{n!}[\omega_s(t)-\omega_0]^n - i\omega_s(t)t\right\}. \quad (1)$$

Using this method the instantaneous frequency ω_s can be determined by equating the phase to zero. We do this assuming that the second-order term is much greater than other terms:

$$\frac{d\varphi}{d\omega} \approx \varphi_2(\omega-\omega_0) - t = 0 \Rightarrow \omega_s(t) = \omega_0 + \frac{t}{\varphi_2}. \quad (2)$$

Then, we substitute formula (2) into expression (1) to obtain the approximate expression:

$$E(t) \propto E_\omega\left(\omega_0 + \frac{t}{\varphi_2}\right)\exp\left[i\sum_{n>2}\frac{\varphi_n}{n!}\left(\frac{t}{\varphi_2}\right)^n - i\omega_0 t - i\frac{t^2}{2\varphi_2}\right]. \quad (3)$$

We multiply expression (3) for the pump wave by the complex-conjugate expression (3) for the amplified wave (see the truncated equations in Refs [17, 18]) to arrive at the expression proportional to the derivative of the idler wave. Equating the result to the relation (3) for the idler wave and then equating the coefficients for the same powers of t, we derive the final expression:

$$\varphi_{in} = \begin{cases} \left(\varphi_{p2}^{-1} - \varphi_{s2}^{-1}\right)^{-1}, & n = 2, \\ \left(\varphi_{p2}^{-1} - \varphi_{s2}^{-1}\right)^{-n}\left[\dfrac{\varphi_{pn}}{\varphi_{p2}^n} - \dfrac{\varphi_{sn}}{\varphi_{s2}^n}\right], & n > 2. \end{cases} \quad (4)$$

Assuming sequential parametric amplification of the idler wave by the signal wave from the previous stage, and assuming that the initial expansion coefficients of their phases of the same order have the same modulus and opposite signs, using (4) we obtain the coefficients presented in Table 5. Note that at the first step, which corresponds to the idler wave (2.24 μm), the odd-numbered phase expansion coefficients are exactly zero. Furthermore, the coefficients of high-order terms decrease much faster than the coefficient of the second-order term, which is due to the denominators in the second expression in the set of expressions (4). The decrease in the coefficient of the second-order term also explains the decrease in the duration of the chirped pulse with an increase in the spectrum width.

Numerical simulations displayed a good convergence of the formulas (Table 5) for stages up to the second, inclusive, to within several percent of the magnitudes of expansion coefficients. For the third stage the accuracy lowers to 10% for φ_2 and to more than 20% for the next expansion coefficients, and for the fourth stage it lowers to 25% and 50%, respectively. The discrepancy with the formulas is attributable to a decrease in the phase expansion coefficients both of the second order, which reduces the overall accuracy of the approximation, and of higher orders, which makes them comparable with the expansion coefficients of the linear dispersion of the medium. If the value of φ_2 is greater, for

Table 5. Coefficients of spectral phase expansions calculated on the basis of Eqns (4).

Stage	Wave	λ_{CM} /μm	φ_2	φ_3	φ_4	φ_5	τ_{chirp} /ps
1 (at input)	Amplified	0.86	φ_2	φ_3	φ_4	φ_5	40
	Idler	1.395	$-\varphi_2$	$-\varphi_3$	$-\varphi_4$	$-\varphi_5$	40
1 (at output)	Amplified	1.395	$-\varphi_2$	$-\varphi_3$	$-\varphi_4$	$-\varphi_5$	38
	Idler	2.224	$\varphi_2/2$	0	$\varphi_4/8$	0	37
2 (at output)	Amplified	2.239	$\varphi_2/2$	0	$\varphi_4/8$	0	33
	Idler	3.665	$-\varphi_2/3$	$-\varphi_3/27$	$-\varphi_4/27$	$-\varphi_5/243$	31
3 (at output)	Amplified	3.587	$-\varphi_2/3$	$-\varphi_3/27$	$-\varphi_4/27$	$-\varphi_5/243$	16
	Idler	6.803	$\varphi_2/5$	$-\varphi_3/125$	$\varphi_4/125$	$\varphi_5/3125$	15
4 (at output)	Amplified	7.453	$\varphi_2/5$	$-\varphi_3/125$	$\varphi_4/125$	$\varphi_5/3125$	9.6
	Idler	5.375	$-\varphi_2/8$	$-\varphi_3/256$	$-\varphi_4/256$	$-\varphi_5/16384$	8.8

example, by an order of magnitude, and if the chirped pulse duration is accordingly longer, the accuracy of the calculation using formula (4) for the last stages will be higher.

Modelling has shown that the characteristic values of the third–fifth order chirp for a grating stretcher do not significantly affect the amplification process. It was found that the spectrum width and the amplified pulse energy change by no more than 0.5%. Formula (4) allows one to analytically calculate the compressor parameters for compressing amplified pulses after any stage. However, as shown above, numerical simulation gives more accurate values of the φ_n coefficients for achieving the minimum duration.

5. Conclusions

The configuration of mid-IR (1.3–15 μm) optical parametric multistage amplification presented in our work opens up the possibility of producing femtosecond pulses with a duration of one field cycle or shorter. We show that parametric amplification with large non-collinearity angles provides an ultrawide spectral amplification band, as well as the possibility to maximise the efficiency of using nonlinearity and the spatial separation of the amplified beams in a short distance. Analysed for the first time are the phase transfer processes of signal and idler waves in multistage parametric amplification configurations for double-chirped pulses. This permits us to calculate the compressor parameters for compressing the amplified pulses after each amplification stage.

The scheme may be scaled up to multiterawatt power by raising the energies of the output pulses in the 0.86 and 1.359 μm domains, but the scaling is limited by the available apertures of the nonlinear-optical crystals. At the same time, AGGS and AGSe crystal growth technologies are actively developing. The Authors of Ref. [31], for instance, demonstrated the possibility of directed growth of AGSe crystals of a given orientation, which will permit a significant increase in their aperture.

The generation of high-power few-cycle pulses in the range of 7–10 μm using the developed scheme may open the way to the production of zeptosecond pulses by high-order harmonic generation [32]. It should also be noted that research is underway to grow new nonlinear-optical crystals for the IR region with the selected determining properties, as well as with simultaneously high $\chi^{(2)}$ susceptibility and optical breakdown threshold [33]. These research works are at the stage of studying the properties of synthesised crystals, and the prospects for their use in nonlinear optical configurations for generating IR radiation with multiterawatt power will be possible to evaluate after the development of a scalable technology for their growth.

Furthermore, the generation of timed wave packets in different spectral regions, which may be implemented in the configuration discussed in this paper, makes it possible to produce coherent radiation with a complex temporal envelope for the optimisation of attosecond pulse generation, including a radical improvement in the efficiency of high-order harmonic generation [34].

Acknowledgements. This work was supported by the Basic Research Programme of the SB RAS (Project Nos 0307-2017-0011 and 0307-2018-0013).

References

1. Ishii N., Kaneshima K., Kitano K., Kanai T., Watanabe S., Itatani J. *Nat. Commun.*, **5**, 3331 (2014).
2. Xue B., Tamaru Y., Fu Y., Yuan H., Lan P., Mücke O.D., Suda A., Midorikawa K., Takahashi E.J. *Sci. Adv.*, **6**, eaay2802 (2020).
3. Trunov V.I., Frolov S.A., Pestryakov E.V. *Proc. SPIE*, **9680**, 96803N (2015).
4. Fu Y., Midorikawa K., Takahashi E.J. *Sci. Rep.*, **8**, 1 (2018).
5. Fu Y., Nishimura K., Xue B., Suda A., Midorikawa K. *EPJ Web of Conferences*, **205**, 24 (2019).
6. Martin B., Grafenstein L., Griebner U., Elsaesser T. *J. Opt. Soc. Am. B*, **35**, 18 (2018).
7. Sanchez D., Hemmer M., Baudisch M., Cousin S.L., Zawilski K., Schunemann P., Chalus O., Simon-Boisson C., Biegert J. *Optica*, **3**, 147 (2016).
8. Yanchun Y., Chew A., Ren X., Li J., Wang Y., Wu Y., Chang Z. *Sci. Rep.*, **7**, 45794 (2017).
9. Šuminas R., Tamošauskas G., Dubietis A. *Opt. Lett.*, **43**, 235 (2018).
10. Frolov S.A., Trunov V.I., Bagaev S.N. *Quantum Electron.*, **50**, 343 (2020) [*Kvantovaya Elektron.*, **50**, 343 (2020)].
11. Houkun L., Krogen P., Wang Z., Park H., Kroh T., Zawilski K., Schunemann P., et al. *Nat. Commun.*, **8**, 1 (2017).
12. Kun L., Liang H., Wang L., Qu S., Lang T., Li H., Wang Q.J., Zhang Y. *Opt. Lett.*, **44**, 1003 (2019).
13. Zhang Q., Takahashi E.J., Mücke O.D., Lu P., Midorikawa K. *Opt. Express*, **19** (8), 7190 (2011).
14. Fu Y., Takahashi E.J., Zhang Q., Lu P., Midorikawa K. *J. Opt.*, **17** (12), 124001 (2015).
15. Bagaev S.N., Trunov V.I., Pestryakov E.V., Leshchenko V.E., Frolov S.A., Vasil'ev V.A. *Quantum Electron.*, **44**, 415 (2014) [*Kvantovaya Elektron.*, **44**, 415 (2014)].
16. Bagayev S.N., Trunov V.I., Pestryakov E.V., Frolov S.A., Leshchenko V.E., Kokh A.E., Vasiliev V.A. *Laser Phys.*, **24**, 074016 (2014).

17. Frolov S.A., Trunov V.I. *Appl. Opt*., **56**, 6375 (2017).
18. Frolov S.A., Trunov V.I., Pestryakov E.V., Leshchenko V.E. *Quantum Electron*., **43**, 481 (2013) [*Kvantovaya Elektron*., **43**, 481 (2013)].
19. Petrov V. *Opt. Mater*., **34**, 536 (2012).
20. Schunemann P.G., Zawilski K.T., Pollak T.M. *J. Cryst. Growth*, **287**, 248 (2006).
21. Rame J., Petit J., Viana B. *Tech. Dig. Advanced Solid-State Lasers Congress* (Paris, Optical Society of America, 2013) paper AM4A.32.
22. Myronchuk G.L., Lakshminarayana G., Kityk I.V., Fedorchuk A.O., Vlokh R.O., Kozer V.R., Parasyuk O.V., Piasecki M. *Chalcogenide Lett*., **15**, 151 (2018).
23. Petrov V. *Prog. Quantum Electron*., **42**, 1 (2015).
24. Beutler M., Rimke I., Büttner E., Farinello P., Agnesi A., Badikov V., Badikov D., Petrov V. *Opt. Express*, **23**, 2730 (2015).
25. Novák O., Krogen P.R., Kroh T., Mocek T., Kärtner F.X., Hong K.H. *Opt. Lett*., **43**, 1335 (2018).
26. Fu Y., Xue B., Midorikawa K., Takahashi E.J. *Appl. Phys. Lett*., **112**, 241105 (2018).
27. Wang T.J., Major Z., Ahmad I., Trushin S.A., Krausz F., Karsch S., *Appl. Phys., B*, **100**, 207 (2010).
28. Heiner Z., Petrov V., Steinmeyer G., Vrakking M.J.J., Mero M. *Opt. Express*, **26**, 25793 (2018).
29. Shvydkoy D.O., Trunov V.I. *Appl. Phys. B*, **126**, 116 (2020).
30. Shvydkoy D.O., Trunov V.I. *Proc. SPIE*, **11322**, 113220T (2019).
31. Schunemann P.G., Setzler S.D., Pollak T.M. *J. Cryst. Growth*, **211**, 257 (2000).
32. Hernández-García C., Pérez-Hernández J.A., Popmintchev T., Murnane M.M., Kapteyn H.C., Jaron-Becker A., Becker A., Plaja L. *Phys. Rev. Lett*., **111**, 033002 (2013).
33. Brant J.A., Clark D.J., Kim Y.S., Jang J.I., Weiland A., Aitken J.A. *Inorg. Chem*., **54**, 2809 (2015).
34. Huang W., Cirmi G., Moses J., Hong K.H., Bhardwaj S., Birge J.R., Chen L.J., Li E., Eggleton B.J., Cerullo G., Kärtner F.X. *Nat. Photonics*, **5**, 475 (2011).